COMMUNICATIONS MATERIALS

ARTICLE

https://doi.org/10.1038/s43246-020-00071-5 OPEN

Improved gravimetric energy density and cycle life in organic lithium-ion batteries with naphthazarin-based electrode materials

Masaru Yao[1]✉, Noboru Taguchi[1], Hisanori Ando[1], Nobuhiko Takeichi[1] & Tetsu Kiyobayashi[1]

Replacing the scarce metal-based positive electrode materials currently used in rechargeable lithium ion batteries with organic compounds helps address environmental issues and might enhance gravimetric electrochemical capacity. The challenge has been to find organic materials with both high capacity and long-cycle life. Here, we study the naphthazarin (5,8-dihydroxy-1,4-naphthoquinone) skeleton as a high capacity candidate electrode for lithium-ion batteries, showing a multielectron-transfer type redox reaction. We also use electron energy-loss spectroscopy to reveal the reaction stoichiometry during charge/discharge processes. While the lithium salt of naphthazarin itself helped deliver a high initial capacity, its cycle-life was not satisfactory. Instead, a newly synthesized naphthazarin-dimer shows a lengthened cycle-life without sacrificing the initial high capacity of 416 mAh g^{-1} and energy density of 1.1 Wh g^{-1}.

[1] Research Institute of Electrochemical Energy, Department of Energy and Environment, National Institute of Advanced Industrial Science and Technology (AIST), 1-8-31 Midorigaoka, Ikeda, Osaka 563-8577, Japan. ✉email: m.yao@aist.go.jp

Their high energy densities have rendered the lithium ion batteries (LIBs) an indispensable power source in modern life. Among the ever-growing demands for the LIBs is the reduction in the amount of scarce metals, with which the positive electrodes of the current LIBs are heavily loaded. Increasing the energy density is also required to drive electric devices a longer time. As an alternative option to meet these requirements, many redox active organic compounds have been examined as an electrode material[1–15]. The intrinsically heavy metal-free organic compounds have the potential not only to eradicate the environmentally undesirable elements from the electrode, but also to simultaneously increase the gravimetric capacity thanks to their multi-electron transfer type redox reactions. This high gravimetric capacity and a relevant high gravimetric energy density features of such organic compounds would be favorable especially when they are applied to aircraft in which the weight of the batteries do become very important. We have demonstrated in previous studies that a series of low-molecular-weight quinone compounds undergo multi-electron redox reactions leading to high capacities[16,17]; however, it is still challenging to obtain a compound which satisfies both the high capacity and long cycle-life.

In this study, with the objective of a higher capacity, we have focused our attention on the naphthazarin (5,8-dihydroxy-1,4-naphthoquinone) derivatives, in which the benzoquinone moiety is fused with the lithium salt of hydroquinone (NP-Li: **1** in Fig. 1). The conceivable four-electron transfer redox reaction[18] has the theoretical capacity of 531 mAh g^{-1}, which is more than three times the practical capacity of the conventional $LiCoO_2$ (*ca.* 160 mAh g^{-1}) and even higher than the theoretical one of the simplest quinone derivative, 1,4-benzoquinone (496 mAh g^{-1}). While the naphthazarin monomer suffers from a short cycle-life, we have proved that the newly synthesized dimer fused by the dithiin ring (DNP-Li: **2** in Fig. 1) endures longer cycles without impairing its high capacity. Furthermore, we have successfully applied electron energy loss spectroscopy (EELS) to quantitatively analyze the Li ion in the electrode, whereby we are able to understand the reaction stoichiometry.

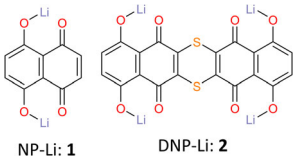

Fig. 1 Chemical structures of the naphthazarin-based organic electrode compounds. Naphthazarin dilithium salt (NP-Li): **1** and tetra lithium salt of the naphthazarin dimer fused by the dithiin ring (DNP-Li): **2**.

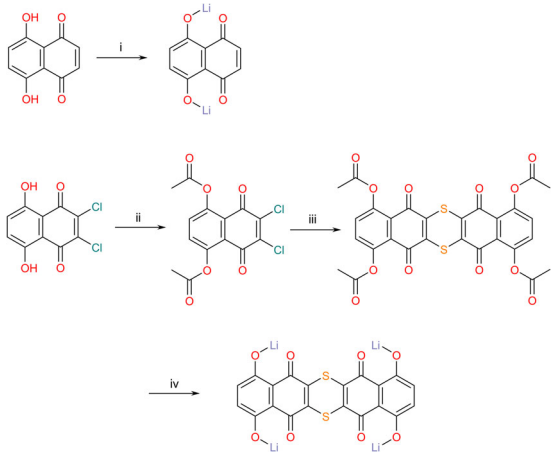

Fig. 2 Synthetic route for the lithium salts of the naphthazarin monomer 1 and the dimer 2. Reagents and conditions: (i) LiOH *aq.*, 50 °C; (ii) acetic anhydride, reflux; (iii) rubeanic acid, TEA/DMF, 50 °C; (iv) LiOH, H_2O/THF, 70 °C.

Results

Synthesis of naphthazarin derivatives. The naphthazarin Li salt (NP-Li: **1**) was prepared by neutralization of naphthazarin with a LiOH *aq.* as described in our previous paper[18]. To synthesize a dimer, we used the dithiin ring, a six-membered ring carrying two sulfur atoms as a linker. The naphthazarin dimer fused by the dithiin ring unit was synthesized from 2,3-dichloronaphthazarin in three steps, Fig. 2. First, the hydroxy groups of naphthazarin were protected by the acetyl group[19], then dimerized by the reaction with rubeanic acid[20] to form the dibenzo[*b*,*i*]thianthrene skeleton. A subsequent hydrolysis and neutralization gave the desired compound (DNP-Li: **2**). The yields at each step were relatively high (>90%). The synthesized **2** is stable upon heating, i.e., the thermal gravimetric analysis (TGA) and differential scanning calorimetry (DSC) showed that its decomposition temperature is close to 400 °C (Supplementary Figs. 1 and 2). A heating treatment at 350 °C for 1 h of **2** did not drastically affect the charge/discharge performance. (A small weight change during heating below 400 °C is considered to reflect the hydrated water release or the decomposition of impurities.)

While the crystal structure of **2** is not clear at present, microcrystals were obtained for the acetyl-protected precursor, of which the SEM analysis indicated that the particles were columnar crystals with smooth surfaces. Although the crystals are small (about 30 μm, Supplementary Fig. 3), one crystallite was large enough to give the X-ray diffractions (Supplementary Fig. 4) that allowed us to solve the crystal structure. The ORTEP drawing, Fig. 3a, suggests that the precursor indeed possesses a dithiin ring and the protective acetyl groups are bonded to the outer side of the molecule. The peripheral acetoxy groups are oriented at an angle almost perpendicular to the naphthazarin plane (84.1°, 84.5°), reflecting the steric effect among these parts. The two naphthazarin and one dithiin rings virtually form a single plane; namely, all the 22 atoms ($C_{20}S_2$) in this ring system are located within 0.011 Å from the mean plane. In the crystal, this molecule stacks one-dimensionally to form a column structure with the mean intermolecular distance of 3.41 Å (Fig. 3b), which is close to the interlayer distance of 3.35 Å for graphite.

The following novel dimer, **2**, does not dissolve in the ordinary solvents (Supplementary Fig. 5), which is important to realize long cycle-life active materials. All the characterization measurements, which can be applied to the analysis of the solid-state compounds, such as MS, IR, elemental analysis, and solid-state ^{13}C-NMR (Supplementary Figs. 6–11), confirm the structure of the present molecule. The SEM image of the pristine powder of **2**, Fig. 3c, suggests that the micron-size crystals have a prismatic structure. The XRD pattern indicates that the powders of **2** are crystalline (Supplementary Fig. 12) and the TEM observation, Fig. 3d, detected a layered pattern with the interval of *ca.* 7 Å, implying a certain ordering of the molecule in the crystal. The fact that this distance is close to the minor axis length of **2** predicted by DFT of 7.6 Å allows us to infer that **2** forms a layered structure in the crystal as sometimes seen for ionic organic compounds[21–23].

Battery performance of the naphthazarin monomer and dimer. As described above, the naphthazarin monomer, **1**, is considered

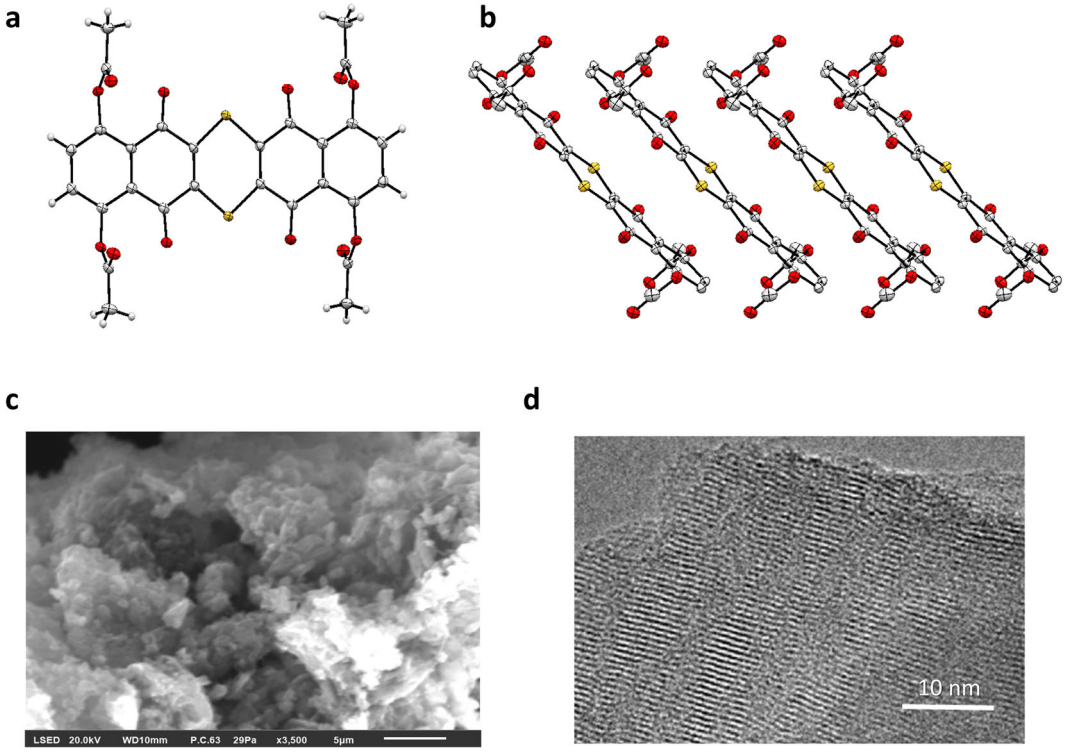

Fig. 3 Characterization of some dimeric derivatives. a, **b**, ORTEP drawing of the acetyl-protected precursor (**a**) and its stacked structure (**b**). Crystal system: monoclinic; Space group: *I2/a* (No. 15); *a*: 20.9463(3) Å; *b*: 4.77582(6) Å; *c*: 24.9250(4) Å; *β*:91.3017(12)°; *Z*: 4; $R_{(I>2\sigma(I))}$: 2.61%; $R_{(all)}$: 2.80%; $wR_{(all)}$: 7.10%; GOF: 1.070; Radiation: Cu *Kα*; Reflection: 7450; *T*: −173 °C. **c**,**d**, Wide field SEM (**c**) and high resolution TEM (**d**) images of the powder of **2**.

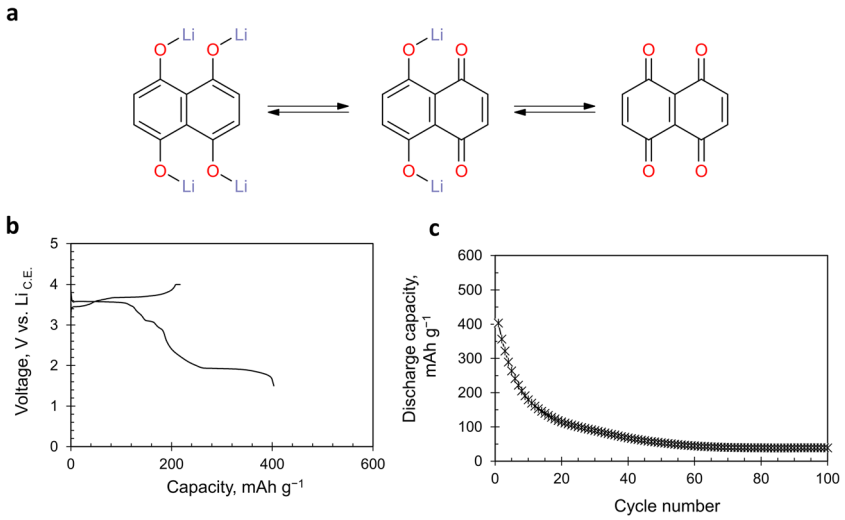

Fig. 4 Battery performance of the electrode using the naphthazarin monomer 1. a, Conceivable charge/discharge reaction of **1**. **b**, **c** Charge/discharge curves (**b**) and cycle-performance (**c**) of the electrode of **1**. (Current density: 20 mA g^{-1}, Temperature: 30 °C).

to show a four-electron transfer type redox reaction (Fig. 4a), which can lead to a high capacity. Figure 4b shows the initial charge and the following discharge curves of the electrode composed of **1**. Since this molecule is in a half-charged state (i.e., the State of Charge (SOC): 50%) at the pristine state, the capacity observed during the first charge process corresponds to half of its full capacity. The following first discharge curve can be roughly divided in two voltage regions. The higher voltage region around 3.5 vs. $Li_{C.E.}$ reflects the reduction (cathodic) reaction of the diquinone (the lithium-free derivative shown on the right side of the redox scheme in Fig. 4a) which should be formed during the first charge process of the naphthazarin lithium salt **1** (dilithium form). The lower voltage region around 2 V vs. $Li_{C.E.}$ corresponds to the further reduction in which the tetra-hydroxy-naphthalene-tetra-lithium salt (shown in the left side of Fig. 4a) is supposed to be formed. The observed capacity of 403 mAh g^{-1} accounts for 76% of the theoretical one, 531 mAh g^{-1}, based on the assumed four-electron redox reaction per molecule. The average discharge voltage of 2.65 V vs. $Li_{C.E.}$ is close to that for the benzoquinone derivatives[16]. This initial behavior implies that the naphthazarin skeleton has the potential to work as a high capacity redox unit. Nevertheless, its cycle stability was poor; namely, as shown in Fig. 4c, the discharge capacity quickly began to drop after the second cycle to eventually decay to 39 mAh g^{-1} after 100 cycles.

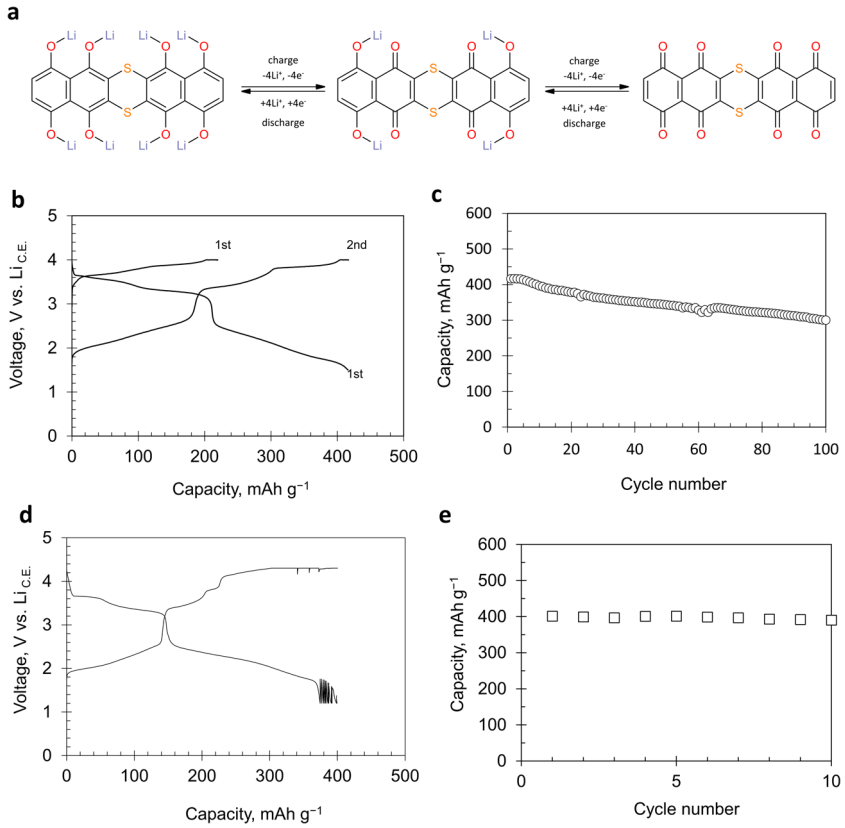

Fig. 5 Battery performance of the electrode using 2. a Conceivable charge/discharge reaction of **2**. **b**, **c** Typical charge/discharge curves during initial cycles (**b**) and cycle-life performance of the electrode incorporating **2** (**c**). (Current density: 20 or 50 mA g^{-1}, Temperature: 30 °C.) **d**, **e** Charge/discharge curves (**d**) and cycle-life performance (**e**) of the high-content (83 wt%) electrode containing **2**. (Current density (discharge): 20–0.5 mA g^{-1}).

This phenomenon is often seen for low-molecular-weight active materials, which is considered to reflect the dissolution of such active materials into the electrolyte solution.

Next, the battery performance of the dimer, **2**, is described. The synthesized dimer, **2**, conceivably undergoes an eight-electron transfer reaction, Fig. 5a, which should lead to the high theoretical capacity of 462 mAh g^{-1}. (The dithiin ring can undergo one electron oxidation reaction at higher potential than the redox of the quinone moieties according to a theoretical calculation. If one can use this reaction, the theoretical capacity would be 520 mAh g^{-1}.) The initial charge/discharge and the following charge curves of the electrode using the dimer **2**, Fig. 5b, are composed of multiple voltage plateau regions, which resemble the shape of those of **1**, though each plateau region is tilted, probably reflecting the enhanced electronic interaction due to the dimerization. The order of the Li^+ to insert to the molecule of **2** is not clear at present. A careful operando XRD measurement and quantum calculation considering the bulk effect would give us a hint for this issue. The electrode made of **2** delivered a high initial capacity, 416 mAh g^{-1}, which is also close to the theoretical value. The average discharge voltage, 2.74 V vs. $Li_{C.E.}$, which exceeds that of the monomer (2.65 V vs. $Li_{C.E.}$) by 0.09 V, translates into the gravimetric energy density of about 1.1 Wh g^{-1}. (Here, the energy density was calculated by multiplying the specific capacity and average voltage.) The obtained value is relatively high compared to the already reported compounds of not only organic[5,24,25] but also inorganic positive electrode materials, except for elemental sulfur. The relatively high specific mass density of this material, 2.1 g cm^{-3}, which is comparable to that of graphite (2.2 g cm^{-3}), leads to the volumetric energy density of 2.3 Wh cm^{-3}, exceeding that of $LiFePO_4$, a material already in actual use (*ca.* 1.8 Wh cm^{-3}). If the full theoretical capacity of **2** is available, the gravimetric and volumetric energy densities would reach 1.3 Wh g^{-1} and 2.6 Wh cm^{-3}, respectively. The rate capability of the electrode using **2** was also examined by discharging at various current densities (Supplementary Fig. 13). Even at 400 mA g^{-1} (~1 C), the capacity was about 300 mAh g^{-1}. This electrode showed a power maximum (14 W g^{-1}) at the current density of around 8 A g^{-1}. This power output is comparable to that of an electrode incorporating a commercially available carbon layer deposited $LiFePO_4$ which has been specially designed for high-power usage. The impedance measurement indicated that the internal resistance of the electrode is small during the middle DOD region as shown in Supplementary Fig. 14. It should be noted that such a high-rate performance can be influenced by many other factors including cell components than the properties of the active material itself; therefore, further discussion is beyond this study. The dimer electrode excels in cycling stability, Fig. 5c; it maintained 300 mAh g^{-1} after 100 cycles, a relatively good performance among the low-molecular-weight quinone derivatives, which tend to leach out into the electrolyte solutions during cycling, resulting in a short cycle-life[16,17,26]. This study demonstrated that the dimerization can limit the dissolution of the active material into the electrolyte to improve the cycle stability. Furthermore, an electrode in which the active material ratio is increased to about 83 wt% was prepared and examined. Many organic active materials often require a large amount of carbon additives to obtain their high capacity values. This extra weight can seriously reduce the capacity value per total weight of the electrode; therefore, reducing the amount of conductive additive, and increasing the ratio of active materials in the electrode are very important to put such organic active

materials into practical use[27]. For this study, the prepared high-content electrode containing **2** showed the very high capacity of 374 mAh g^{-1} at 20 mA g^{-1} and exceeded 400 mAh g^{-1} at the lower current densities despite the fact that the active material ratio was very high (Fig. 5d), which can be a great advantage for its practical application. (The prepared high-content electrode also showed fair cycle stability as shown in Fig. 5e). The charge curves of this high-content electrode apparently differ from those of the low-content one. The cyclic voltammetry showed that the shape of the voltammograms varies depending on the carbon-additive contents in the electrodes (Supplementary Fig. 15a). The shape was also affected by the scan rate especially for the low-carbon content electrodes (Supplementary Fig. 15b). These results imply that the low-carbon content electrode has a high over-voltage and slow kinetics due to the increased internal resistance and uneven distribution of the active material in the electrode. To circumvent these issues, one would need to improve the current collecting ability in the electrode, for example by a carbon coating on the active material powders, specially designed conductive additives[27], etc.

A symmetric full cell using the dimer. The two carbonyl and two hydroxy groups in naphthazarin can undergo reduction and oxidation, respectively. This bipolar characteristic suggests that its lithium salt has the potential to work not only as a positive but also as a negative active material, Fig. 6a. A full cell was tested in which the electrodes of **2** were used as both the positive and negative electrodes. The charge/discharge curves during the initial two cycles, Fig. 6b, have two voltage plateau regions; one is around 1.8 V and the other is around 1.0 V during the discharge process, both of which can be explained by the potential difference between two pairs of two plateaus observed in the half-cell in Fig. 5b. The observed capacity of 189 mAh g^{-1} is close to the theoretical one of 231 mAh g^{-1} under the assumption of a four-electron transfer per molecule. The cell maintained the capacity of 122 mAh g^{-1} after 100 cycles, Fig. 6c. In the literature, one can find only a limited number of symmetric full-cell tests in which the same organic material is used in both electrodes[28,29]. Using the identical electrode as both the negative and positive electrode would partially contribute to reducing the battery cost.

Charge/discharge mechanism of the naphthazarin derivatives. In order to obtain an insight into the reaction mechanism of the naphthazarin derivatives, ex-situ ^{1}H-NMR spectroscopy was first used to evaluate the chemical structural change during the charge and discharge processes of **1**. Figure 7a compares the NMR spectra of the extracts from the electrode in the charged and discharged states with those of compounds chemically oxidized and reduced. The spectrum of the fully charged state shifts downfield from the initial compound **1** and agrees with its chemically oxidized state, i.e., diquinone. On the other hand, the extract from the fully discharged electrode has a signal shifted upfield from **1** and agrees with that of its chemically reduced compound, the tetrahydroxy naphthalene lithium salt. The NMR signals simulated by a quantum chemistry calculation qualitatively agrees with these experimental results; *viz*., the calculation predicts a downfield 0.24 ppm shift and an upfield 1.1 ppm shift from **1** for diquinone and the tetraanionic state, respectively. Incidentally, we found that the polarization function must be added to the hydrogen atom to reproduce the spectra, implying the important role played by the higher orbitals of the hydrogen atom when dealing with the ^{1}H-NMR. These observations substantiate the fact that the four-electron transfer in Fig. 4a indeed takes place in the electrode.

Furthermore, the charge/discharge mechanism of **2** during cycling was also examined by an ex-situ TEM-EELS technique for the electrode of **2**, since the above-mentioned NMR technique is not suitable for **2** due to its low solubility in the ordinary organic solvents. While the carrier ion in the rechargeable lithium batteries is usually Li^+, some organic positive electrode active materials reported for the lithium system accommodate anions[1,3,8] such as PF_6^- or ClO_4^- instead of Li^+. Therefore, identifying the carrier ions is important in understanding the charge and discharge mechanism to develop a practical battery. In this study, we successfully identified the carrier ion to be Li^+ and determined its stoichiometry in the electrode of **2**. The EELS signal from the Li atom changed according to the SOC of the electrodes which were charged or discharged to specific states, Fig. 7b. The quantitative relation was derived in such a way that the mean peak area for the initial state was normalized to 4.0 to which the area for the charged and discharged electrodes was compared; namely, the Li content per molecule decreased to 0.7

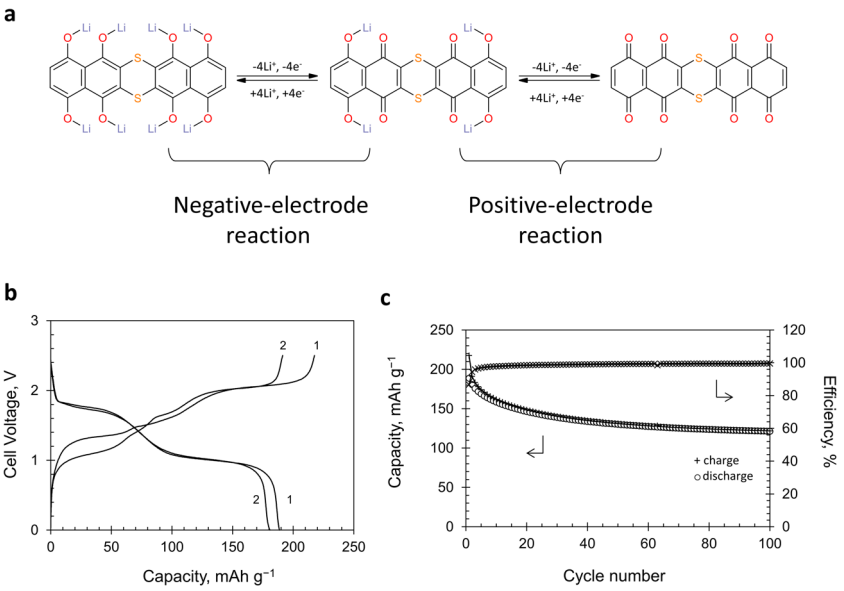

Fig. 6 Charge/discharge behavior of the symmetric full cell using 2 as both the positive and negative electrodes. a Redox reaction of **2** in both electrodes. **b** Charge/discharge curves of the full cell. **c** Cycle-life performance of the full cell.

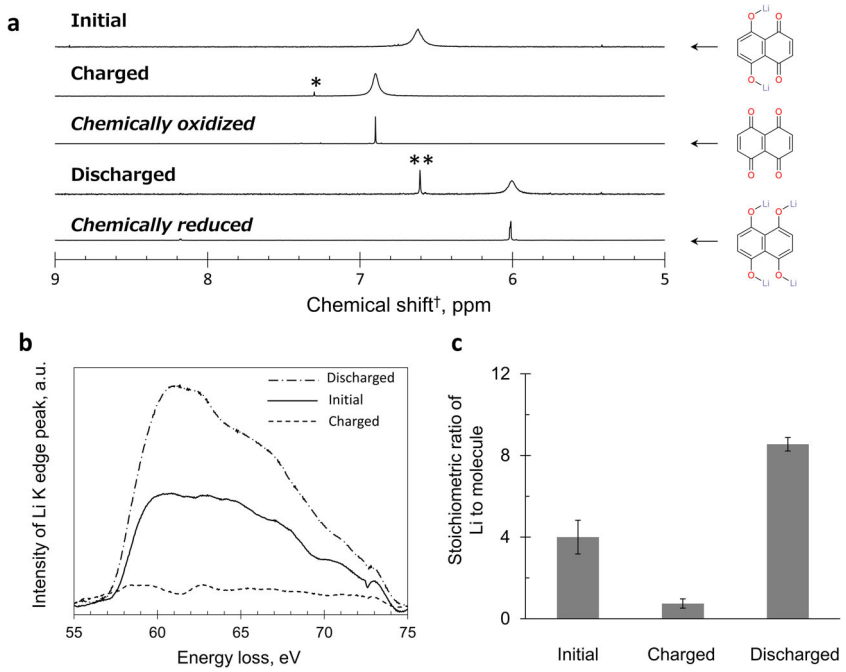

Fig. 7 Charge/discharge mechanism analysis of the electrodes using the naphthazarin monomer 1 and the dimer 2. a ^{1}H-NMR analysis for **1** during the charge/discharge processes. The signals with '*' and '**' indicate the minor components of the partially reduced and oxidized states, naphthazarin hydroxy form and **1**, respectively. †The signal positions were calibrated with respect to those of **1** in DMSO-d_6. **b**, **c** EELS spectra from the Li *K*-edge (**b**) and stoichiometric ratio of Li to **2** with standard deviation bars (**c**).

(2) after the first charge and increased to 8.5(2) after the subsequent discharge as shown in Fig. 7c. This result proves that the charge carrier is Li^+ with the reaction stoichiometry that the molecule releases four Li^+ ions during the initial charge and accommodates eight Li^+ ions after a full discharge. This observation corroborates the total eight-electron redox reaction of the molecule accompanied by the eight-lithium storage and release.

In order to understand the charge/discharge behaviors of the naphthazarin derivatives, their molecular orbitals were calculated by DFT for **1** and **2**. In addition, a model compound, **2′**, in which two naphthazarin moieties are fused with a benzo ring was compared to clarify the effect of the dithiin ring of **2**. As for the small naphthazarin analogs, the electronic state of their HOMO and LUMO should be relevant when discussing the electrochemical properties and considering their redox mechanism. In addition to these frontier orbitals, the NLUMO and NHOMO should also be evaluated for the dimers because of the orbital splitting caused by the fusion. Figure 8a depicts the related molecular orbitals of the optimized structures of **1** and **2**, and benzo-fused dimer, **2′**, along with the energy diagrams. In each molecule, the molecular orbitals are delocalized over the molecules based on their π-characteristics.

Whereas the contours of the orbitals resemble **2** and **2′**, their energy levels are influenced in a different fashion by the ring fusion. The average energy of the redox-relating orbitals (NLUMO, LUMO, HOMO, and NHOMO) of **2′** is located at 0.2 eV higher than that of **1**. Taking the accrual redox potential of **1** into consideration, the average potential of **2′** would be 2.48 V vs. Li^+/Li, which is lower than that of **1**. As is often observed, the fusion by the sp^2-type unsaturated rings tend to lower the average discharge voltage probably due to the strong interaction between the redox-relating orbitals, with which our calculation for **2′** agrees. On the contrary, the effect of the dithiin-ring fusion on the energy level is limited and opposite to that of the benzo-ring, for which the saturated sp^3-type sulfur atom that blocks the delocalization of the π-electron is responsible; i.e., the average energy of these MOs of **2** is 0.1 eV lower than that of **1**. The estimated average potential of **2** from this calculation is 2.71 V vs. Li^+/Li, which well agrees with the experimentally observed discharge voltage of 2.74 V vs. $Li_{C.E.}$ for **2**. Using the dithiin ring to fuse organic molecules is thus an effective way to increase its molecular weight without decreasing the discharge voltage.

How the intermolecular interaction in the crystal is increased by the dimerization was also calculated[30], in which the fully charged (oxidized) molecule was examined because its Li-free state allows us to optimize the structure without introducing the ambiguity caused by the assumptions in the Li position. The optimization gave parallel displaced stacking structures for the fully charged states of **1** and **2**, Fig. 8b. The off-set π-stacking is typical in π-conjugated polycyclic molecules, thus validating the present calculation. The intermolecular binding energy of the oxidized **1** and **2** was calculated to be 27 and 81 kJ mol^{-1}, respectively. While the former value is typical for such stacked small molecules, the latter is very high for molecules associated by the van der Waals interaction. Incidentally, a hypothetical trimer, **3**, in which three naphthodiquinone moieties are fused by two dithiin rings, was also calculated to be in a stacked structure with the intermolecular interaction of 127 kJ mol^{-1}, about five-fold greater than that of **1**. Furthermore, the solvation energy for these fully oxidized compounds in sulfolane was calculated at the same level to be 35, 69, and 101 kJ mol^{-1} for the monomer, dimer and trimer, respectively, summarized in Fig. 8c along with the stacking energy. The solvation energy for the monomer is greater than the binding energy via the π-stacking, which indicates that the monomer prefers to be dissolved in the solvent. On the other hand, the trend is opposite for the dimer and trimer; i.e., the binding energy for these compounds exceeds their solvation energy. In addition, the energy difference for the trimer is greater than that of the dimer. This calculation indicates that these oligomers would hardly dissolve in the solvent.

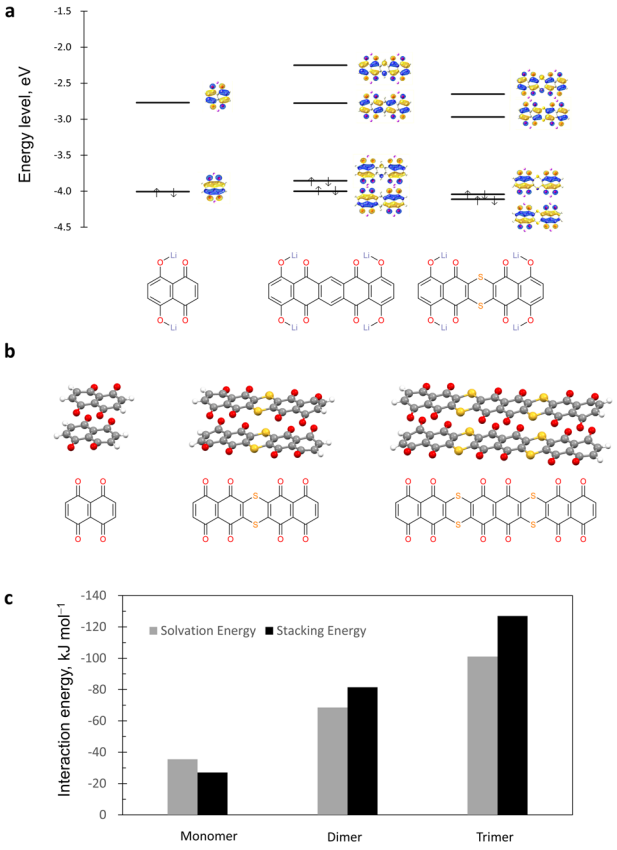

Fig. 8 Quantum chemistry calculation for naphthazarin derivatives. a The calculated energy level diagrams of some MOs of the lithium salt of the naphthazarin-monomer (**1**), a benzo-fused dimer (**2′**), and the dithiin-fused dimer (**2**). **b** The calculated stacking structures of the fully charged states of **1**, **2**, and a hypothetical trimer **3**. **c** Comparison of stacking energy and solvation energy calculated for the fully charged state of **1**, **2**, and **3**.

Discussion

The initial discharge capacities and the average voltages are very similar for the monomer **1** and dimer **2**; i.e., 403 and 416 mAh g^{-1} 2.6 and 2.7 V vs. $Li_{C.E.}$, respectively. The gravimetric energy density exceeds 1.0 Wh g^{-1} for both **1** and **2**, which is relatively high compared to those of the reported electrode materials of not only organic compounds but also inorganic counterparts such as $LiCoO_2$, $Li(Ni\text{-}Mn\text{-}Co)O_2$ or $LiFePO_4$ which range from 0.5 to 0.7 Wh g^{-1} [31]. Unlike the ordinary quinones, the naphthazarin derivatives can be prepared in the pristine states that contain lithium ions, which eliminates the necessity to pre-dope Li when manufacturing the full cell, thus making naphthazarin an attractive candidate as a high energy-density active material. The dimer **2** underwent many more cycles than the monomer **1**.

Not only is the chemical stability of the material important for the long cycle-life, but also the dissolution of the organic compound into the electrolyte solution causes the capacity decay, which is responsible for the poor cycling performance of the low molecular weight organic active materials as already reported. In the wake of our previous investigation in a series of alkoxy benzoquinone analogs, we have established the trend that the lower the solubility in the solvent, the longer the cycle-life[26]. While polymerization has been regarded as a method to suppress the dissolution, it often significantly diminishes the capacity from the theoretical one, as exemplified in our previous study in which the utilization ratio of a naphthazarin polymer was not satisfactory during the charge and discharge[32]. Introducing polar substituents is another way to prevent the molecules from dissolving into the polar solvent, though at the expense of the decrease in the theoretical capacity per se due to the extra weight of those substituents[14,33].

While the direct fusion of the redox-active moiety is reported to be effective in extending the cycle-life along with maintaining a high utilization ratio[17], it also lowers the voltage due to the strong intramolecular orbital interaction. Although the lithium salt of either monomer **1** or dimer **2** hardly dissolves into the organic solvent, the fully charged diquinone state of **1** is quite soluble, for instance, in chloroform, benzene, acetonitrile, DMSO, etc.[15,34–36]. The dissolution of the diquinone state of **1** was confirmed by the color change of the electrolyte solution after cycling in this study. A theoretical calculation suggested that the intermolecular interaction in **2**, 81 kJ mol^{-1}, is threefold greater than that in **1** and exceeds that of the hydrogen bond, 10–40 kJ mol^{-1}, which is considered a relatively strong interaction. The calculation predicts the intermolecular interaction of a hypothetical trimer **3** to be 127 kJ mol^{-1}, rivaling that of the covalent bond, 100–300 kJ mol^{-1}. In addition, the solvation energy calculation gave a further insight about the solubility of these compounds. Similar to the trend of the binding energy, the solvation energy also increases as the molecular size increases. The stacking energy exceeds the solvation energy when oligomerized. This observation indicates that such high molecular weight oligomers energetically prefer to be in a bulk environment rather than to be an isolated solute in the solvent. Although at a finite temperature the entropy would lever the equilibrium towards the solution state, the quantum chemistry calculation, which reflects the state at 0 K, suggests that the increase in the molecular weight due to the oligomerization renders the solid state stable. Thus we speculate that the solubility of the fully charged **2**, which is still unknown, would be significantly lower than that of **1** thanks to the stronger intermolecular interaction. This study demonstrated that the dimerization or trimerization by the dithiin ring is very effective in enhancing the intermolecular attraction to overcome the solvation energy so that the dissolution is sufficiently limited to prolong the cycle-life without affecting the energy density. Thus we speculate that the solubility of the fully charged **2**, which is still unknown, would be significantly lower than that of **1** thanks to the stronger intermolecular interaction.

In summary, as a redox active organic unit with a high energy density, we focused our attention on the naphthazarin (5,8-dihydroxy-1,4-naphthoquinone) skeleton, of which the theoretical capacity is *ca.* 500 mAh g^{-1}, based on its four-electron transfer reaction. The lithium salt of the monomer, **1**, delivered a high capacity and high energy density (403 mAh g^{-1} and 1.1 Wh g^{-1}) during the initial discharge process; however, the capacity quickly decreased upon cycling. To improve the cycle-stability, a naphthazarin dimer, **2**, fused by the dithiin ring was newly synthesized in order to compare its battery performance to that of the monomer, **1**. The electrode made of **2** initially delivered a high capacity and gravimetric energy density (416 mAh g^{-1} and 1.1 Wh g^{-1}, respectively) and maintained about 300 mAh g^{-1} after 100 cycles. Also, **2** showed the high capacity of 374 mA h g^{-1} even when the active material content ratio in the electrode was increase to more than 80%. A quantum chemistry calculation indicated that the dimerization of the naphthazarin unit by the sp^3-based dithiin ring would not lower the potential. The intermolecular attraction through the π-π interaction in the dimer was calculated to be stronger than the solvation interaction, which should alleviate the dissolution of the dimer into the electrolyte solution. We successfully applied the NMR and EELS methods to prove that the charge carrier is indeed Li by determining the reaction stoichiometry. Fusing the multi-electron transfer units by a saturated ring would serve as a guide for designing a new organic active material that fulfills both the high energy density and long cycle-life.

Methods

Materials. 5,8-Dihydroxy-1,4-naphthoquinone (Alfa Aesar), 2,3-dichloro-5,8-dihydroxy-1,4-naphthoquinone (Tokyo Chemical Industry), and the other chemicals used for the synthesis were purchased and used without further purification. The naphthazarin dilithium salt (**1**) was prepared by the neutralization of naphthazarin with lithium hydroxide. The synthesized compounds were characterized by the liquid type ^{1}H-NMR and ^{13}C-NMR (JEOL, JHM-ECS series, $\nu(^1H) = 400$ MHz), infrared (IR), and mass apparatus (Waters, ACQUITY SQD mass spectrometer) equipped with an atmospheric solids analysis (ASAP) or electrospray ionization (ESI) probes, and melting point measurement (Stanford Research Systems, OptiMelt MPA-100). A solid-state MAS-^{13}C-NMR (JEOL, JNM-ECX400) with CPMAS and DDMAS modes was also used to characterize the final compound **2**. The specific weight (density) of **2** was measured by gas displacement pycnometry (Micromeritics Instruments Corp., AccuPyc series). The analytical data (MS, IR, NMR, SEM, EDX, XRD, etc.) are listed in the Supplementary information.

Synthesis of the naphthazarin dimer 2. 2,3-Dichloro-5,8-dihydroxy-1,4-naphthoquinone 3.0 g (12 mmol) was dissolved in 75 mL of acetic anhydride and the solution was refluxed for 8 h. After cooling, the precipitate was filtered and washed to give 3.7 g of a yellow solid of 5,8-diacetoxy-2,3-dichloro-1,4-naphthoquinone[19]. Yield: 92%. M.p.: 237 °C. ASAP-MS, *m/z*: calcd. for $C_{14}H_8{}^{35}Cl_2O_6$, $C_{14}H_8{}^{35}Cl^{37}ClO_6$: 342, 344; Found: 343, 345 $[M + H]^+$. IR, cm^{-1}: 1764 (acetyl C=O), 1684 (quinone C=O). ^{1}H-NMR (400 MHz, $CDCl_3$): δ 7.45 (s, 2H, peripheral C*H*), 2.46 (s, 6H, acetyl CH_3). ^{13}C-NMR (400 MHz, $CDCl_3$) (Supplementary Fig. 16): δ 174.0 (*C*=O), 169.0 (*C*=O), 148.5 (*C*–O), 143.2 (*C*–Cl), 131.9 (*C*–H), 123.6 (bridgehead *C*), 21.0 (CH_3).

To the solution of 5,8-diacetoxy-2,3-dichloro-1,4-naphthoquinone (0.85 g, 2.5 mmol) and rubeanic acid (0.17 g, 1.4 mmol) in 13 mL of *N*,*N*-dimethylformamide was added a small amount of triethylamine. The reaction mixture was stirred for 10 h at 50 °C. After cooling to room temperature, the precipitate was filtered and washed with water to give 0.72 g of 1,4,8,11-tetraacetoxydibenzo[*b*,*i*]thianthrene-5,7,12,14-tetrone as a red solid. Yield: 96%. M.p.: 314 °C. ESI-MS($CHCl_3$), *m/z*: calcd. for $C_{28}H_{16}O_{12}S_2$: 608; Found: 608 $[M]^+$. IR, cm^{-1}: 1765 (acetyl C=O), 1655 (quinone C=O). ^{1}H-NMR (DMSO-d_6): δ 7.65 (s, 4H, peripheral C*H*), 2.33 (s, 12H, acetyl CH_3). ^{13}C-NMR (DMSO-d_6) (Supplementary Fig. 16): δ 175.2 (*C*=O), 168.6 (*C*=O), 147.3 (*C*–O), 139.2 (*C*–S), 131.8 (*C*–H), 123.1 (bridgehead *C*), 20.5 (CH_3). E.A. calcd. for $C_{28}H_{16}O_{12}S_2$: C, 55.26; H, 2.65; S, 10.54%. Found: C, 54.79; H, 2.50; S, 10.92%.

1,4,8,11-Tetraacetoxydibenzo[*b*,*i*]thianthrene-5,7,12,14-tetrone (0.82 g, 1.4 mmol) was treated in a lithium hydroxide solution in a mixed solvent of water (10 mL) and tetrahydrofuran (50 mL), and the resulting solution was stirred for 1 h at 70 °C. After evaporation of the solvent, the residue was washed with ethanol to give 0.60 g of 1,4,8,11-tetrahydroxydibenzo[*b*,*i*]thianthrene-5,7,12,14-tetrone tetra lithium salt (**2**) as a bluish purple solid. Yield: 97%. M.p.: >400 °C. ASAP-MS (hydroxy deriv.), *m/z*: calcd. for $C_{20}H_8O_8S_2$: 440; Found: 441 $[M + H]^+$. IR, cm^{-1}: 1635 (aromatic C=C stretch), 1549 (C=O/CO$^-$ sym. stretch), ~1400 (C=O/CO$^-$ asym. stretch). ^{1}H-NMR (DMSO-d_6): δ 6.54 (s, 4H, peripheral C*H*). ^{1}H-NMR (solid, CP-MAS): δ 6.65 (s, 4H, peripheral C*H*). ^{1}H-NMR (DMSO-d_6) (hydroxy deriv.): δ 11.92 (s, 4H, phenolic O*H*), 7.47 (s, 4H, peripheral C*H*). ^{13}C-NMR (solid, CP-MAS): δ 179.3 (*C*–O), 168.3 (*C*–O), 138.1 (*C*–H and *C*–S), 116.9 (bridgehead *C*). (Other measurements with different contact times and the measurement using the dipolar decoupling mode imply that the peak at 138.1 ppm is an overlapped one.) E.A. calcd. for $C_{20}H_4Li_4O_8S_2{\cdot}½H_2O$: C, 50.77; H, 1.07. Found: C, 50.39; H, 0.71. E.A. calcd. for $C_{20}H_8O_8S_2{\cdot}½H_2O$ (hydroxy deriv.): C, 53.99; H, 1.93; S, 14.41%. Found: C, 53.95; H, 1.97; S, 14.15%. Specific weight (density): 2.1 g cm^{-3}.

Single crystal analysis. Single crystals of the acetyl-protected precursor of **2** suitable for X-ray analysis were obtained by a slow cooling of its hot *N*-methylpyrrolidone solution. A red prism crystal (0.26 × 0.04 × 0.03 mm) was selected and mounted in a loop. All measurements were made by using a Rigaku XtaLAB PRO MM007 diffractometer (Rigaku) with multi-layer mirror monochromated Cu *K*α radiation ($\lambda = 1.54184$ Å). Data were collected and processed using CrysAlisPro (Data Collection and Processing Software, Rigaku Corp.). The structure was solved by direct methods (SHELXT ver. Ver. 2014/5)[37] and expanded using Fourier techniques. All calculations were performed using a crystallographic software package (CrystalStructure, Rigaku Corp.) except for refinement, which was performed using SHELXL ver. 2014/7[38].

Preparation of electrodes and cells. As a positive-electrode, a composite sheet composed of an organic active material powder, acetylene black as the conductive additive, and polytetrafluoroethylene as the binder was prepared by mixing them in the weight ratio of 4:5:1 in a mortar. The sheet (~0.8 cm^2, ∅~10 mm) was then pressed onto a mesh-type aluminum current collector. The amount of active material was approximately 3.00 mg per electrode. The battery performance of the organic compounds as positive electrode active materials was examined by assembling IEC R2032 coin-type cells with a lithium metal negative-electrode, separator, and about 0.2 mL of the electrolyte solution of lithium bis(trifluoromethanesulfonyl)imide (LiTFSI) / sulfolane (2.4 mol kg^{-1}).

Electrochemical measurements. Cyclic voltammetry (CV) was applied to the prepared cells using electrochemical analyzers (Solartron SI1280B and ALS 610E). The voltammogram was recorded at the scan rates of 0.2, 0.1, and 0.05 mV/s in the potential range of 1.2–4.2 vs. $Li_{C.E.}$ at 30 °C. The electrochemical impedance of the cells was recorded with the same electrochemical analyzer at the various depth of discharge. The frequency ranges from 1×10^{-2} to 1×10^5 Hz with an alternative current signal of 0.1 mA amplitude.

The prepared coin-type cells were galvanostatically charged at the current density of 50 mA g^{-1} for the active materials to the upper limit of the voltage of 4.0 V vs. $Li_{C.E.}$ followed by a one-hour potentiostatic charge, then galvanostatically discharged at 20 mA g^{-1} to the lower voltage limit of 1.5 V vs. $Li_{C.E.}$ The charge/discharge measurement was performed by a battery evaluation system (ABE system, Electrofield Co., Ltd.) at 30 °C. In this paper, the obtained capacities are expressed in terms of mass of the active material in the positive electrode.

^{1}H-NMR spectroscopy for the monomer 1. The chemical structure change in the electrode during the charge/discharge process of **1** was measured ex situ by ^{1}H-NMR spectroscopy. For this measurement, a solution of lithium perchlorate/dimethyl carbonate (3 mol kg^{-1}) and LiTFSI / tetrahydofuran (3 mol kg^{-1}) were used as the electrolyte solutions to obtain the charged and discharged states, respectively. First, the cell at a given state of charge and discharge was disassembled under an inert atmosphere. The electrode was taken out and dried under reduced pressure. The redox active components were extracted by immersing each electrode in $(CD_3)_2SO$ or D_2O, and the ^{1}H nucleus in the solutions was measured. The initial state of **1** shows a single peak at 6.61 ppm vs. tetramethylsilane (TMS, $(CH_3)_4Si$) in $(CD_3)_2SO$ and 6.90 ppm vs. sodium 3-(trimethylsilyl)propionate-2,2,3,3-d_4 (TSP, $(CH_3)_3Si(CD_2)_2COONa$) in D_2O. The chemical shift position of **1** in the former system (DMSO solution) was used as a reference to correct the solvent effect. The chemically oxidized compound of **1**, 1,4,5,8-naphthodiquinone, was prepared using a hypervalent iodine-type oxidation reagent, [bis(trifluoroacetoxy)iodo]benzene, according to the literature[35]. The chemically reduced species, 1,4,5,8-tetrahydroxynaphthalene tetra lithium salt, was prepared by reacting **1** and $Na_2S_2O_4$ in D_2O with an excess amount of LiOH. This reduced tetralithium salt shows a peak at 6.29 ppm vs. TSP-d_4 in D_2O without any corrections. To compare the chemical shift change of the above mentioned states dissolved in different solvents, the peak of **1** was used as an internal reference.

Theoretical calculations. To obtain the energy level of the molecular orbitals (MOs), the density functional theory calculation using a popular basis set of 6-31G (d) and a functional of BLYP were used. In this calculation, a self-consistent reaction field (SCRF) with the conductor-like polarizable continuum model (CPCM) was applied to simulate a bulk environment. The redox average potential of the above-treated molecules was empirically estimated by considering the difference between the calculated average energy level of the redox-related orbitals of each molecule and that of the monomer as a potential deviation from the experimentally obtained average value for **1** (2.65 V vs. Li$^+$/Li). As for the NMR simulation, a single point calculation using a basis set of 6-31+G(d,p) and the CSGT method was used for the structure which was optimized at the b3lyp/6-31G (d) level. To estimate the intermolecular binding energy of **1** and **2**, their stacking structures were optimized by the same basis set using the hybrid DFT functional of BHandH[39], which is often applied for a system including non-covalent interactions, followed by the single point calculation based on the Møller-Plesset perturbation theory (MP2) by the same basis set. To take the solvation effect into consideration, the self-consistent polarizable continuum model (SC-PCM) was applied to our molecular system. A single point calculation in sulfolane was conducted at the MP2/6-31G(d) level for the optimized structures. All the quantum chemistry calculations were performed using the GAUSSIAN 03, 09, and 16 program packages[40] and the calculated MOs were visualized by Gauss View 3.0[41].

TEM-EELS analysis for the dimer 2. An ex-situ electron energy-loss spectroscopy (EELS) measurement was used to analyze the charge/discharge mechanism of the electrode using a scanning transmission electron microscope (TEM) (Titan^3 G2 60-300) equipped with an EELS apparatus (GIF-Quantum, Gatan, Inc.) at an acceleration voltage of 300 kV. For this analysis, some cells composed of the positive electrode using **2** and the lithium metal negative electrode with a 1 mol kg^{-1} lithium hexafluorophosphate/tetrahydofuran electrolyte solution were prepared. The electrodes after the charge/discharge test were removed from the cells and washed with degassed dimethoxyethane to dissolve out the electrolyte salt before the measurement. The sample powder for the TEM analysis was obtained from the electrode and directly dispersed on a holey carbon film supported on a Cu mesh. The change in the lithium ion concentration of the electrode was measured using EELS. The EELS spectra were measured at the areas where the sulfur atom signals from the molecular structure of **2** were previously observed by the EDX analysis. After eliminating the effect of multiple scattering by Fourier-log deconvolution, each spectrum was filtered by the Savitzky-Golay smoothing, then the exponential background subtraction method was used to extract the integrated Li K-edge intensity. To compare the Li K-edge intensity of each sample, the signal was normalized with the relative thickness and detector counts obtained from electrons transmitted through the vacuum region. The normalized lithium peak strength

values were then converted to the amounts of the lithium atom per molecule using the peak strength of the initial state molecule of **2** which contains four lithium atoms as a reference.

Data availability

The data that support the findings of this study are available from the corresponding author (M.Y.) upon reasonable request.

Received: 24 October 2019; Accepted: 7 September 2020;
Published online: 02 October 2020

References

1. Novák, P., Müller, K., Santhanam, K. S. V. & Hass, O. Electrochemically active polymers for rechargeable batteries. *Chem. Rev.* **97**, 207–281 (1997).
2. Armand, M. & Tarascon, J. M. Building better batteries. *Nature* **451**, 652–657 (2008).
3. Nakahara, K. et al. Rechargeable batteries with organic radical cathode. *Chem. Phys. Lett.* **359**, 351–354 (2002).
4. Yoshikawa, H., Kazama, C., Awaga, K., Satoh, M. & Wada, J. Rechargeable molecular cluster batteries. *Chem. Commun.* **30**, 3169–3170 (2007).
5. Chen, H. et al. From biomass to a renewable LixC6O6 organic electrode for sustainable Li-ion batteries. *ChemSusChem* **1**, 348–355 (2008).
6. Song, Z., Zhan, H. & Zhou, Y. Anthraquinone based polymer as high performance cathode material for rechargeable lithium batteries. *Chem. Commun.* **4**, 448–450 (2009).
7. Jing, Y., Liang, Y., Gheytani, S. & Yao, Y. Cross-conjugated oligomeric quinones for high performance organic batteries. *Nano Energy* **37**, 46–52 (2017).
8. Janoschka, T., Hager, M. D. & Schubert, U. S. Powering up the future: radical polymers for battery applications. *Adv. Mater.* **24**, 6397–6409 (2012).
9. Liang, Y. L., Tao, Z. L. & Chen, J. Organic electrode materials for rechargeable lithium batteries. *Adv. Energy Mater* **2**, 742–769 (2012).
10. Poizot, P. & Dolhem, F. Clean energy new deal for a sustainable world: from non-CO_2 generating energy sources to greener electrochemical storage devices. *Energy Environ. Sci.* **4**, 2003–2019 (2011).
11. Matsunaga, T., Kubota, T., Sugimoto, T. & Satoh, M. High-performance lithium secondary batteries using cathode active materials of triquinoxalinylenes exhibiting six electron migration. *Chem. Lett.* **40**, 750–752 (2011).
12. Inatomi, Y., Hojo, N., Yamamoto, T., Watanabe, S. & Misaki, Y. Construction of rechargeable batteries using multifused tetrathiafulvalene systems as cathode materials. *ChemPlusChem* **77**, 973–976 (2012).
13. Morita, Y. et al. Organic tailored batteries materials using stable open-shell molecules with degenerate frontier orbitals. *Nat. Mater.* **10**, 947–951 (2011).
14. Shimizu, A. et al. Introduction of two lithiooxycarbonyl groups enhances cyclability of lithium batteries with organic cathode materials. *J. Power Sources* **260**, 211–217 (2014).
15. Yokoji, T., Matsubara, H. & Satoh, M. High-capacity organic cathode active materials of 2,2′-bis-p-benzoquinone derivatives for rechargeable batteries. *J. Mater. Chem. A* **2**, 19347–19354 (2014).
16. Yao, M. et al. High-capacity organic positive-electrode material based on a benzoquinone derivative for use in rechargeable lithium batteries. *J. Power Sources* **195**, 8336–8340 (2010).
17. Yao, M., Yamazaki, S., Senoh, H., Sakai, T. & Kiyobayashi, T. Crystalline polycyclic quinone derivatives as organic positive electrode materials for use in rechargeable lithium batteries. *Mater. Sci. Eng. B* **177**, 483–487 (2012).
18. Yao, M. et al. Rechargeable organic batteries using chloro-substituted naphthazarin derivatives as positive electrode materials. *J. Mat. Sci.* **52**, 12401–12408 (2017).
19. Horowska, B. et al. Synthesis and cytotoxic activity of aziridinyl- 1,4-naphthoquinones. *Eur. J. Med. Chem.* **23**, 91–96 (1988).
20. Fenical, W., Jensen, P. R., La Clair, J. J., Trzoss, L. & Fukuda, T. Seriniquinones, melanoma-specific anticancer agents; (The regents of the university of California). Patent: WO2014/18919 A1 (2014).
21. Yao, M. et al. Indigo carmine: an organic crystal as a positive-electrode material for rechargeable sodium batteries. *Sci. Rep.* **4**, 3650 (2014).
22. Kaduk, J. A. Terephthalate salts: salts of monopositive cations. *Acta Cryst. B* **56**, 474–485 (2000).
23. Ogihara, N. et al. Organic dicarboxylate negative electrode materials with remarkably small strain for high-voltage bipolar batteries. *Angew. Chem. Int. Ed.* **126**, 11651–11656 (2014).
24. Zhu, Z. Q. et al. All-solid-state lithium organic battery with composite polymer electrolyte and pillar[5]quinone cathode. *J. Am. Chem. Soc.* **136**, 16461–16464 (2014).
25. Lu, Y. et al. Cyclohexanehexone with ultrahigh capacity as cathode materials for lithium-ion batteries. *Angew. Chem. Int. Ed.* **58**, 7020–7024 (2019).
26. Yao, M., Ando, H. & Kiyobayashi, T. Dialkoxybenzoquinone-type active materials for rechargeable lithium batteries: the effect of the alkoxy group length on the cycle-stability. *Energy Procedia* **34**, 880–887 (2013).
27. Kato, M., Sano, H., Kiyobayashi, T., Takeichi, N. & Yao, M. Conductive polymer binder and separator for high-energy-density lithium organic battery. *MRS Commun.* **9**, 979–984 (2019).
28. Zhu, L. M., Lei, A. W., Cao, Y. L., Ai, X. P. & Yang, H. X. An all-organic rechargeable battery using bipolar polyparaphenylene as a redox-active cathode and anode. *Chem. Commun.* **49**, 567–569 (2013).
29. Wang, S. et al. Organic $Li_4C_8H_2O_6$ nanosheets for lithium-ion batteries. *Nano Lett.* **139**, 4404–4409 (2013).
30. Yao, M., Sano, H., Ando, H., Kiyobayashi, T. & Takeichi, N. Anthraquinone-based oligomer as a long cycle-life organic electrode material for use in rechargeable batteries. *ChemPhysChem* **20**, 967–971 (2019).
31. Brodd, R. J. (ed.) Batteries for Sustainability: Selected Entries from the Encyclopedia of Sustainability Science and Technology, Chapter 2, *Battery Cathodes*, Doeff, M. M. (Springer, New York, 2013).
32. Yao, M. et al. Improving the cycle-life of naphthoquinone-based active materials by their polymerization for rechargeable organic batteries. *Energy Procedia* **89**, 213–221 (2016).
33. Yao, M. et al. Indigo dye as a positive-electrode material for rechargeable lithium batteries. *Chem. Lett.* **39**, 950–952 (2010).
34. Zwirchmayr, N. S. et al. Degradation of the cellulosic key chromophore 5,8-Dihydroxy-[1,4]-naphthoquinone by hydrogen peroxide under alkaline conditions. *J. Org. Chem.* **82**, 11558–11565 (2017).
35. Yoshino, S., Hayakawa, K. & Kanematsu, K. Reagent design and study of p-benzoquinone derivatives. Site-selective cycloaddition reaction of diquinones and photochemical cage formation of the adducts. *J. Org. Chem* **46**, 3841–3846 (1981).
36. Hayakawa, K., Aso, M. & Kanematsu, K. Site-selective Diels-Alder reactions of 1,4,5,8-naphthodiquinones with anthracenes and successively with cyclopentadiene: electronic effects vs. steric effects. *J. Org. Chem.* **50**, 2036–2040 (1985).
37. Sheldrick, G. M. SHELXT: Integrating space group determination and structure solution. *Acta Cryst. A* **70**, C1437 (2014).
38. Sheldrick, G. M. A short history of SHELX. *Acta Cryst. A* **64**, 112–122 (2008).
39. Zhao, Y. & Truhlar, D. G. Density functionals for noncovalent interaction energies of biological importance. *J. Chem. Theory Comput.* **3**, 289–300 (2007).
40. Frisch, M. J. et al. Gaussian 03, Revision E.01 (2004), Gaussian 09, Revision C.01 (2010), Gaussian 16, Revision B.01 (2016), Gaussian, Inc., Wallingford, CT (2016).
41. Dennington, R. II. et al. GaussView, Version 4.1.2, Semichem, Inc., Shawnee Mission, KS. (2003).

Acknowledgements

We appreciate the cluster computing for the quantum chemistry calculations by Dr. Hiroyuki Ozaki, AIST. We also thank Ms. Miho Araki, AIST, for her technical support. This work is partially supported by a project commissioned by the New Energy and Industrial Technology Development Organization (NEDO).

Author contributions

M.Y. conceived the project, carried out the experiments, and prepared the manuscript. N.Taguchi carried out the TEM-EELS spectroscopy. H.A. supported the molecular design of the active materials. N.Takeichi supported the crystallographic analysis. T.K. helped to advance this study and partially wrote the manuscript.

Competing interests

The authors declare no competing interests.

Additional information

Supplementary information is available for this paper at https://doi.org/10.1038/s43246-020-00071-5.

Correspondence and requests for materials should be addressed to M.Y.

Reprints and permission information is available at http://www.nature.com/reprints

Publisher's note Springer Nature remains neutral with regard to jurisdictional claims in published maps and institutional affiliations.